NASA TECHNICAL NOTE

NASA TN D-4847

NASA TN D-4847

ENTRIES FROM EARTH ORBIT THAT SIMULATE ACCELERATION STRESSES OF MANNED PLANETARY MISSIONS

by Frederick G. Edwards

Ames Research Center
Moffett Field, Calif.

NATIONAL AERONAUTICS AND SPACE ADMINISTRATION • WASHINGTON, D. C. • OCTOBER 1968

ENTRIES FROM EARTH ORBIT THAT SIMULATE ACCELERATION STRESSES OF MANNED PLANETARY MISSIONS

By Frederick G. Edwards

Ames Research Center
Moffett Field, Calif.

NATIONAL AERONAUTICS AND SPACE ADMINISTRATION

For sale by the Clearinghouse for Federal Scientific and Technical Information
Springfield, Virginia 22151 – CFSTI price $3.00

TABLE OF CONTENTS

ENTRIES FROM EARTH ORBIT THAT SIMULATE ACCELERATION STRESSES OF MANNED PLANETARY MISSIONS

By Frederick G. Edwards

Ames Research Center

SUMMARY

The ability to duplicate the acceleration stress during a portion of the earth return of a planetary mission vehicle by appropriate control of an earth orbital vehicle is investigated. The results show that during the entry of an orbital spacecraft it is possible to approximately match the acceleration profile corresponding to the initial dive, the capture maneuver, and part of a constant altitude deceleration phase of a planetary mission return entry. A two-step approach to the solution is examined: The analytical step results in a closed-form approximate solution for the lift control. An analog computer simulation of the entries uses results from the analytical step and gives a more precise solution for the control. It also permits an evaluation of the cost to the earth entry vehicle in terms of the aerodynamic heating, range capability, and retro velocity requirements.

Emphasis is placed on simulating the planetary mission entry at twice orbital velocity, but the results also apply to entry at other supercircular velocities. An Apollo-type lifting entry vehicle was used for the example entries presented.

INTRODUCTION

The long duration missions to the planets would require astronauts to endure far longer periods of weightlessness (300 to 600 days) and higher reentry acceleration levels (10 g and greater) than has been experienced in past earth orbital missions. If the present man-system relationship is maintained, the astronaut will be required to monitor, guide, and control during entry from these missions. The effects of these extended missions and, in particular, the weightless environment on his ability to tolerate high entry stresses and at the same time perform control functions must be investigated prior to the planetary missions.

Entry from long duration earth orbit missions provides opportunities for studying performance of astronauts after they have been exposed to extended periods in a weightless environment. This report indicates a means whereby earth orbital spacecraft may be used during the entry phase to give meaningful data on the effects of the mission environment on the performance of the astronaut during planetary entry; the technique is to control an earth orbital vehicle during entry so as to duplicate a planetary mission entry acceleration-time profile.

The investigation initially considers the flight dynamics of a planetary mission return vehicle (to be called the reference vehicle), followed by a discussion of the general character of the entry of an earth orbital vehicle (to be called the flight vehicle) when it is controlled to duplicate the planetary mission entry acceleration profile. An approximate equation is developed for the required lift control. Numerical results are obtained from the approximate equation and from a more complete analog computer simulation of the trajectory motions. The effects of acceleration control on the vehicle range capability, aerodynamic heating, and retro velocity increment are determined. A roll-modulated lifting capsule (Apollo) is the spacecraft considered in this study.

SYMBOLS

$\bar{A}_t$ total acceleration, g

C_D drag coefficient, $\frac{D}{(1/2)\rho V^2 S}$

C_L lift coefficient, $\frac{L}{(1/2)\rho V^2 S}$

D drag force, N

g local value of gravity acceleration, m/sec^2

h altitude, m

H total integrated heat load, J/m^2

K_1, K_2 control equation gain constants

L lift force, N

m mass of vehicle, kg

$\dot{q}$ heating rate per unit area, W/m^2

r distance from planet center, m

S reference area for drag and lift coefficients, m^2

S_D downrange distance traveled, km

S_X crossrange distance traveled, km

t time, sec

u circumferential velocity component normal to radius vector, m/sec

u_c circular orbital velocity $\sqrt{gr}$, m/sec

$\bar{u}$ dimensionless velocity ratio $\frac{u}{u_c}$

V resultant velocity $\sqrt{u^2 + w^2}$, m/sec

$\bar{V}$ $\frac{V}{u_c}$

$\Delta\bar{V}$ dimensionless change from initial velocity, $\frac{V_i - V}{\sqrt{gr}}$

$\bar{V}_I$ dimensionless velocity at peak acceleration

w vertical velocity component (along direction of radius vector), m/sec

X_h, Y_h, Z_h physical components of external force, N

Z dimensionless function of $\bar{V}$ given by $\rho\bar{V}\frac{C_D S}{2m}\sqrt{\frac{r}{\beta}}$

β atmospheric scale height, 1/m

γ flight-path angle given by arc tan $\left(\frac{-w}{u}\right)$

η retro thrust vector direction, deg

ρ atmospheric density, kg/m^3

τ dimensionless time, $\sqrt{\frac{g_o}{r_o}}\,t$

φ roll angle, deg

ψ_h lateral deflection angle, deg

Subscripts

com command

nom nominal

ref reference (time function)

o reference (constant value)

1 flight vehicle (initial velocity = 1)

2 reference vehicle (initial velocity = 2)

f final value

i initial value

I value at maximum acceleration

v vertical components

Superscripts

($\dot{}$) differentiation with respect to time

($'$) differentiation with respect to velocity

($\bar{}$) dimensionless quantity

ANALYSIS

General Remarks

This section will discuss the control required, during the atmosphere entry of an earth orbital mission vehicle, to duplicate the acceleration time history during the atmosphere entry of a planetary mission vehicle. A two-step approach is presented. The initial step considers only one component of the entry vehicle motion and leads to an approximate but useful analytical solution. A second step, employing an analog simulation which includes three degrees of vehicle translational motion and one degree of body rotational motion, uses the approximate results from the first step to obtain a more precise solution.

Planetary return (reference vehicle).- The trajectory for a planetary mission return (fig. 1(a)) is assumed to have an entry velocity twice the local satellite velocity. The particular entry shown is one of several types that could be considered and is referred to as a constant altitude entry. To achieve a successful entry the vehicle must enter within the safe corridor between the undershoot and overshoot boundaries of figure 1(a). During the initial dive into the atmosphere the vehicle acceleration increases. At maximum acceleration (pull out) the entry control system (either manned or automatic) is required to perform a "capture" maneuver to insure that the vehicle does not skip out of the atmosphere or dive in to such a degree that destructive acceleration forces build up. In figure 1(a) the vehicle enters near the undershoot boundary. It is stressed in reference 1 that entry near this boundary presents a critical control problem. The vehicle lift vector will be initially full up to insure that the maximum acceleration limit is not exceeded, then,

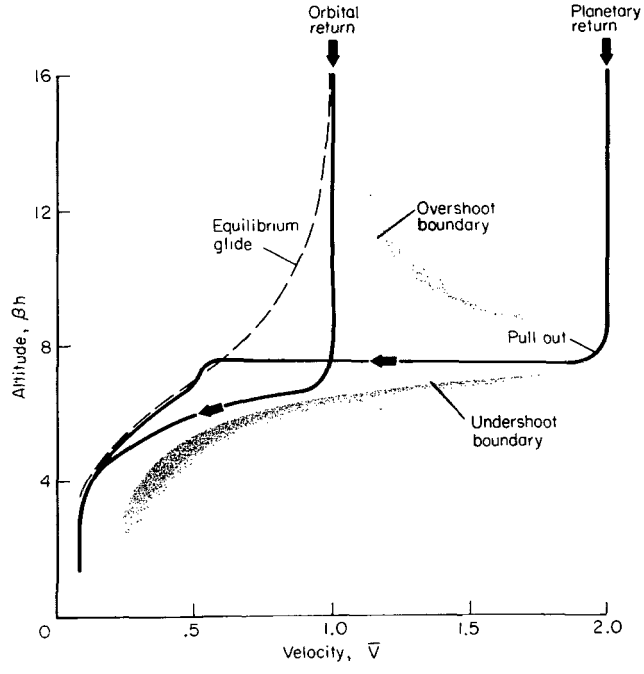

(a) βh vs. $\bar{V}$

Figure 1.- Typical earth entry trajectories for planetary and earth orbital mission vehicles.

at peak g, the vehicle is rolled over so that lift and gravity forces balance the centrifugal force. The next portion of the entry is a constant altitude deceleration phase until sufficient lift can no longer be generated, at which time an equilibrium glide with lift vector full up is flown to landing.

Orbital return (flight vehicle).- The entry trajectory for return from an earth orbital mission (fig. 1(a)) is the particular one that duplicates the acceleration time history for the planetary mission return vehicle. A comparison of the altitude velocity profiles indicates how this match is achieved.

The orbital return vehicle dives to a lower altitude (higher atmospheric density) than the planetary mission return vehicle, and after pull out, pulls down into the atmosphere at an increasingly greater rate as the velocity decays. At each instant when the accelerations along the trajectories are equal, the velocity of the planetary return vehicle will exceed that of the orbital return vehicle. It should be clear that in order for the aerodynamic accelerations to be equal for the two vehicles, the effect of the higher velocity of the planetary return vehicle is being compensated by flying the orbital vehicle at a lower altitude where the atmospheric density is greater. With this technique, the dynamic pressures $[(1/2)\rho V^2]$ for the two vehicles are equivalent. A more direct comparison of the two entry trajectories is shown in figure 1(b), where the two entry trajectories presented in figure 1(a) are now plotted as a function of a new variable $\Delta\bar{V}$, the total velocity change.[1] (In this plot the trajectories proceed toward the right whereas in figure 1(a) they proceeded toward the left.) In figure 1(a), the two trajectories started at different velocities ($(\bar{V}_1)_i = 1.0$, $(\bar{V}_2)_i = 2.0$) and proceeded to zero velocity at the terminal point. In figure 1(b), they start at the same point, $\Delta\bar{V} = 0$, and end at different points ($(\Delta\bar{V}_1)_f = 1.0$, $(\Delta\bar{V}_2)_f = 2.0$). The difference in altitude between the two entry trajectories is more readily apparent in this figure than

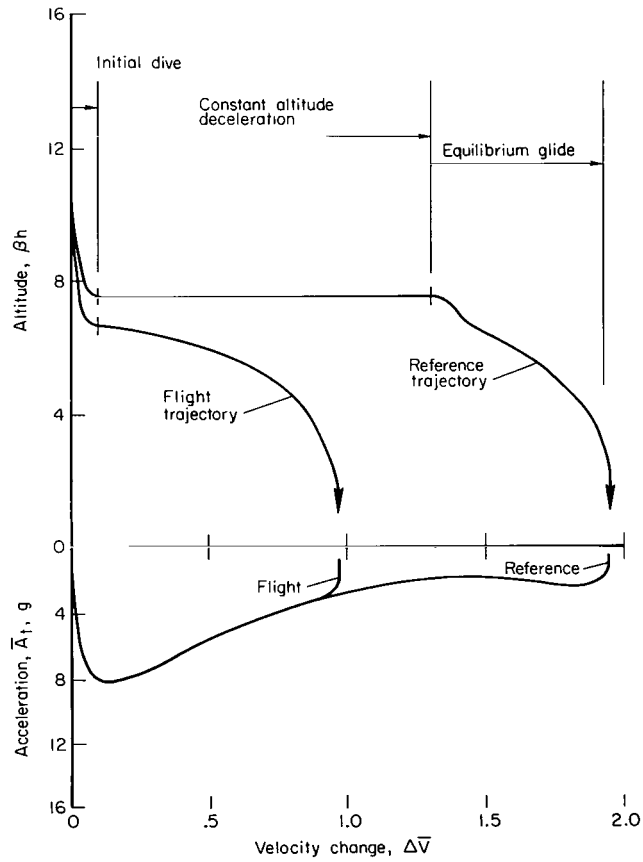

(b) βh vs. $\Delta\bar{V}$

Figure 1.- Concluded.

[1]The difference between the initial velocity of the vehicle and the velocity at a point along the trajectory ($\Delta\bar{V} = \bar{V}_i - \bar{V}$) will be equivalent at equal times for both vehicles if the acceleration profiles are matched. A further discussion of $\Delta\bar{V}$ will appear later in the text.

in figure 1(a). In the lower part of figure 1(b), traces of the total acceleration for the two entry trajectories are presented. Note that the accelerations are equal during the range of $\Delta\bar{V}$ from $0 < \Delta\bar{V} < 1.0$, causing the two plots to appear as a single trace. It is during this increment in $\Delta\bar{V}$ that it is feasible to match the acceleration profiles.

Assumptions

The entry vehicle assumed for this study was a blunt-faced lifting capsule trimmed at the appropriate angle of attack to give a desired L/D. This trim condition is set prior to entry by offsetting the center of mass from the center line of the vehicle. During the actual flight there is no direct control of the magnitude of the lift. The direction of the lift vector is controlled by rolling the vehicle about the velocity vector, giving rise to components of lift, and thus control, in the vertical and lateral directions.

It was assumed that the vehicle aerodynamic coefficients did not vary with Mach number and Reynolds number and that the L/D and ballistic coefficients were only functions of trim angle of attack. These aerodynamic coefficients are given in table I as a function of trim angle of attack.

The vehicle is assumed to enter the atmosphere of a nonrotating cylindrical earth under the influence of aerodynamic and gravitational forces. (An exponential approximation for the 1962 ICAO standard atmosphere is used throughout.) The differential equations describing the vehicle motions during entry are found by summing the accelerations in the vertical, horizontal, and lateral directions at an arbitrary point along the trajectory. The following nonlinear differential equations have been derived in references 2 and 3:

TABLE I.- AERODYNAMIC PARAMETERS FOR SIMULATED VEHICLE.

α, deg	L/D	m/C_DS, kg/m^2
0	0	269
6	0.10	273
15	.25	293
31	.50	391
47	.70	742

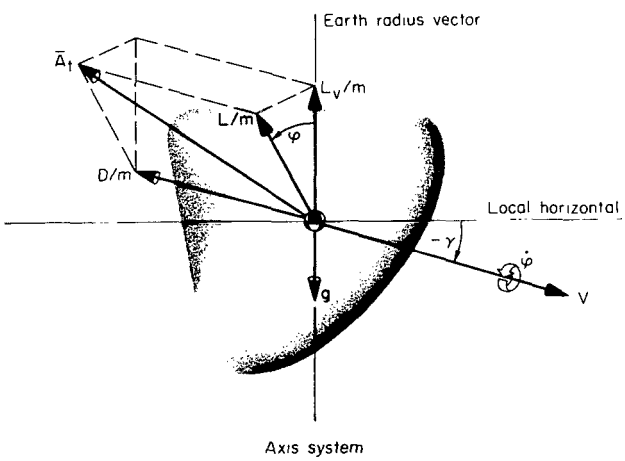

Axis system

$$-\frac{d^2h}{dt^2} - g + \frac{V^2\cos^2\gamma}{r} = \frac{D}{m}\left[\sin\gamma - \left(\frac{L}{D}\right)_V \cos\gamma\right] \qquad (1)$$

$$\frac{d^2S_D}{dt^2} + \frac{V\cos\gamma}{r}\frac{dh}{dt} = -\frac{D}{m}\left[\left(\frac{L}{D}\right)_V \sin\gamma + \cos\gamma\right] \qquad (2)$$

$$\frac{d^2S_X}{dt^2} = \frac{L}{m}\cos\varphi \qquad (3)$$

In this study, as noted previously, solutions are obtained in two steps. Initially, only motion in the vertical direction is considered and equations (2) and (3) are disregarded. An approximate but useful solution is obtained for the vehicle $(L/D)_V$ time profile. The second step of the approach considers all three equations of motion. These are programmed in a modified form and solved using an analog computer simulation. In addition to the $(L/D)_V$ time profile, more extensive results are obtained from this step of the approach.

Control Technique

In this study, an orbital mission return vehicle is controlled in a closed-loop manner during entry to match its flight trajectory variables to the corresponding reference trajectory variables. The reference trajectory variables are those generated during the entry of a planetary mission return vehicle. The variables controlled are the acceleration and the rate of change of acceleration. The control equation

$$\varphi_{com}(t) = \varphi_{nom}(t) + K_1[\bar{A}_{t_{flt}}(t) - \bar{A}_{t_{ref}}(t)] + K_2[\dot{\bar{A}}_{t_{flt}}(t) - \dot{\bar{A}}_{t_{ref}}(t)] \tag{4}$$

is solved continuously during the flight trajectory to determine the value of the control $\varphi_{com}(t)$ required to match the acceleration along the flight and reference trajectories. The terms K_1 and K_2 are constant feedback gains in equation (4). The term $\varphi_{nom}(t)$ is the nominal roll-angle profile along the flight trajectory. This is not equal to the nominal roll-angle profile of the reference trajectory because the initial velocity of the flight trajectory is only half the velocity of the reference trajectory. Although the acceleration profiles for the two trajectories can be identical over a portion of the entry, the control profiles required to achieve this identity will be quite different because of the difference in velocity that exists throughout the portion of the entry where an acceleration match is achieved. Consequently, to proceed with the analog solution, the nominal control profile for the flight trajectory must be determined with sufficient accuracy so that the linearized control equation is valid.

Since the reference trajectory nominal profile ($(L/D)_{ZV}$ versus velocity) and the initial velocity for the two trajectories are known, the corresponding flight trajectory control profile can be determined. It will be shown that an analytical approach results in a closed-form approximate solution for the flight vehicle control profile and allows the use of the linearized control equation in the analog computer approach to finding a more precise solution to the control profile.

Analytic Approach

To determine the proper trajectory control, during the entry of an earth orbit mission vehicle, to match the acceleration profile of a planetary entry

vehicle we shall initially use an approximate but direct method of evaluating the control. The two entry vehicles may have dissimilar aerodynamic and mass characteristics but the total accelerations at an arbitrary instant of time must be equal. Thus, to indicate the variables that influence the match:

$$\bar{A}_{t_1} \equiv \bar{A}_{t_2}$$

or

$$\left(\frac{C_D S}{mg}\right)_1 \sqrt{1 + \left(\frac{L}{D}\right)_1^2}\ \frac{1}{2}\rho_1 V_1^2 = \left(\frac{C_D S}{mg}\right)_2 \sqrt{1 + \left(\frac{L}{D}\right)_2^2}\ \frac{1}{2}\rho_2 V_2^2 \tag{5}$$

where subscript 1 refers to the vehicle entering at local satellite velocity and subscript 2 refers to a planetary return entry at twice local satellite velocity. Equation (5) may be expressed as the difference in altitude between the two entry trajectories at each instant of time (which is necessary in order that their accelerations be equal) by assuming an exponential variation of density with altitude ($\rho = \rho_o e^{-\beta h}$). The resulting expression is

$$h_2 - h_1 = \frac{2}{\beta} \ln \frac{V_2}{V_1} + \frac{1}{\beta} \ln \left[\frac{(C_D S/mg)_2}{(C_D S/mg)_1} \sqrt{\frac{1 + (L/D)_2^2}{1 + (L/D)_1^2}} \right] \tag{6}$$

Equation (6) indicates how the altitude profile of the two entry trajectories should differ as a function of the velocity ratio V_2/V_1 and the aerodynamic and mass characteristics of the vehicles. The second term on the right is constant during entry; thus, the altitude difference varies exponentially with velocity ratio only. This exponential variation is apparent in figure 1(b) for that portion of the orbital return trajectory (after pull out) corresponding to the constant altitude portion of the planetary entry trajectory.

It may be noted that equation (6) could be a solution to the differential equation of motion (eq. (1)), except that the independent variable is velocity instead of time (as in eq. (1)), and the dependent variable is the difference in altitude rather than altitude directly. If the two equations were compatible, the conditions under which equation (6) would be a solution to the differential equation (1) could be determined by directly substituting the solution into the differential equation and determining the values of $(L/D)_V$ required to solve the resulting equation. Assuming for the moment that in equation (6) the reference altitude profile (h_2 vs. V_2) is known, we shall check to see for what conditions a solution is obtained. First, the independent variable must be changed so that the differential equation and its solution correspond. The independent variable chosen will be neither the time nor velocity, as in equations (1) and (6), but the new variable (designated the dimensionless total velocity change) defined as

$$\Delta\bar{V} = \bar{V}_i - \bar{V} \tag{7}$$

where $\bar{V}_i$ is the initial velocity of the vehicle, $\bar{V}$, the velocity at any time along the entry trajectory, and $\Delta\bar{V}$, the difference between these two values. It is proposed that the values of this new variable will be common to both the reference and flight trajectories, in other words, the total changes in velocity at a corresponding time along the trajectories will be equal if the total acceleration profiles are precisely matched. This requires that the integrals of the two total acceleration profiles be equal:

$$\Delta\bar{V} = \int_0^{\tau} \bar{A}_{t_1}\, d\tau' = \int_0^{\tau} \bar{A}_{t_2}\, d\tau' \tag{8}$$

Actually, equation (8) is only approximately true. The conditions under which it is used are presented in appendix A.

Introducing the new variable $\Delta\bar{V}$ into equation (1) and making the small-angle approximation $\cos\gamma = 1$ and $\sin\gamma = \gamma$ results in the simplified expression

$$-\frac{d(\bar{V}\gamma)}{d\Delta\bar{V}} = \frac{1 - \bar{V}^2}{\bar{A}_t/\sqrt{1 + (L/D)^2}} + \gamma - \left(\frac{L}{D}\right)_V \tag{9}$$

where the rate of climb, $\bar{V}\gamma$, has been substituted for its equivalent, $\frac{1}{\sqrt{gr}}\frac{dh}{dt}$. The control variable to be evaluated, $(L/D)_V$, is the vertical component of the total lift-to-drag ratio of the vehicle.

In equation (9) the derivative term is evaluated by differentiating equation (6), a solution to the differential equation. Differentiating with respect to $\Delta\bar{V}$ and substituting in terms of the rate of climb variable $\bar{V}_1\gamma_1$ yields an expression for the flight-path angle γ_1:

$$\bar{V}_1\gamma_1 = \bar{V}_2\gamma_2\sqrt{\frac{1 + (L/D)_2^2}{1 + (L/D)_1^2}} - \frac{2\bar{A}_t}{\beta r\bar{V}_1\bar{V}_2} \tag{10}$$

After a second differentiation,

$$\frac{d\bar{V}_1\gamma_1}{d\Delta\bar{V}} = \frac{d\bar{V}_2\gamma_2}{d\Delta\bar{V}}\sqrt{\frac{1 + (L/D)_2^2}{1 + (L/D)_1^2}} - \frac{2\bar{A}_t}{\beta r\bar{V}_1\bar{V}_2}\left[\frac{1}{\bar{V}_1} - \frac{1}{\bar{V}_2} - \frac{\beta r\bar{V}_2\gamma_2}{\bar{A}_t/\sqrt{1 + (L/D)_2^2}}\right] \tag{11}$$

where subscripts 1 and 2 correspond to the values for the flight and reference vehicle, respectively. The total acceleration $\bar{A}_t$ has no subscript since it

is equivalent for both vehicles. Equations (10) and (11) are substituted directly into the differential equation (9), which is solved for the required value of $(L/D)_{1v}$ which makes equation (6) a solution of equation (9). The result is:

$$\left(\frac{L}{D}\right)_{1v} = \frac{1 - \bar{V}_1^2}{\bar{A}_t/\sqrt{1 + (L/D)_1^2}} + \sqrt{\frac{1 + (L/D)_2^2}{1 + (L/D)_1^2}}\left[\left(\frac{L}{D}\right)_{2v} - \frac{1 - \bar{V}_2^2}{\bar{A}_t/\sqrt{1 + (L/D)_2^2}}\right]$$

$$+ \frac{\gamma_2}{\bar{V}_1}\sqrt{\frac{1 + (L/D)_2^2}{1 + (L/D)_1^2}}\left[\bar{V}_2 - \bar{V}_1 + 2\sqrt{1 + (L/D)_1^2}\right] - \frac{2\bar{A}_t(2\bar{V}_2 - \bar{V}_1)}{\beta r(\bar{V}_1\bar{V}_2)^2} \qquad (12)$$

Substituting for the velocities $\bar{V}_1$ and $\bar{V}_2$ in terms of the common variable $\Delta\bar{V}$ and the initial velocities $(\bar{V}_1)_i = 1$ and $(\bar{V}_2)_i = 2$ gives the expression for the vehicle control:

$$\left(\frac{L}{D}\right)_{1v} = \frac{2\Delta\bar{V} - \Delta\bar{V}^2}{\bar{A}_t/\sqrt{1 + (L/D)_1^2}}$$

$$+ \sqrt{\frac{1 + (L/D)_2^2}{1 + (L/D)_1^2}}\left[\left(\frac{L}{D}\right)_{2v} - \frac{4\Delta\bar{V} - \Delta\bar{V}^2 - 3}{\bar{A}_t/\sqrt{1 + (L/D)_2^2}} + \frac{\gamma_2(1 + 2\sqrt{1 + (L/D)_2^2}}{(1 - \Delta\bar{V})}\right]$$

$$- \frac{2\bar{A}_t(3 - \Delta\bar{V})}{\beta r[(1 - \Delta\bar{V})(2 - \Delta\bar{V})]^2} \qquad (13)$$

In equation (13) the lift required for control of the flight vehicle is related to the lift characteristics of both the flight and reference vehicle and the trajectory parameters of the reference vehicle only. The control is a direct function of the vertical component of the L/D of the reference vehicle, $(L/D)_{2v}$, the L/D of the reference and flight vehicles, the integral of the total acceleration $\Delta\bar{V}$, the magnitude of the acceleration, $\bar{A}_t$, and an indirect function of the rate of change of acceleration through the flight-path angle, γ_2. Although it is not apparent at this point in the discussion, all of these parameters are known quantities. Thus, we have determined that equation (6) will be a solution to the differential equation if the vertical component of the lift vector varies as specified by equation (13). Equation (13) is then the closed-form approximate solution for the flight vehicle control problem. In order to solve equation (13) quantitatively, the reference trajectory must be specified in terms of the variables $(L/D)_{2v}$, $\bar{A}_t$, and γ_2 as a function of the independent variable $\Delta\bar{V}$. It shall now be indicated how these quantities may be determined and a numerical solution obtained.

The altitude versus $\Delta\bar{V}$ profile for the reference trajectory (fig. 1(b)) is conveniently divided into three distinct segments. The initial dive into the atmosphere up to the point of pull out is the first phase. The constant altitude portion is the second phase, followed by the third, designated an equilibrium glide. Our interest will be in duplicating the acceleration profile of the first segment and as much as possible of the second phase. The reference variables for these two segments will be specified separately.

Initial dive phase.- The initial dive into the atmosphere may be considered that portion of the trajectory from atmospheric encounter (i.e., $\bar{A}_t = 0.05$ g) until maximum acceleration. This portion of the trajectory has been solved in closed form for restricted cases by Gazley, Loh, Lees, and others and, in a more general form, by Chapman. Chapman (ref. 2) reduces the two basic differential equations for longitudinal motions (eqs. (1) and (2)) to a single approximate equation. This single equation is a nonlinear second-order differential equation in terms of a generalized dependent variable Z and the independent variable velocity, $\bar{u}$. Although Chapman's equation requires numerical machine calculations, the general results obtained apply to problems involving a range of body shapes, mg/C_DS, and planetary atmospheres. A Set of precomputed entry trajectories, presented in terms of generalized Z functions as well as the more useful values of $\bar{A}_t$, γ, and $\bar{V}$, is presented in tabular form in reference 4 for several different initial velocities and L/D values. The values from these tables may be used successfully as reference trajectory variables for the initial dive into the atmosphere. The acceleration, flight-path angle, and velocity for an initial velocity of $\bar{V}_i = 2.0$ and a specified $(L/D)_{2V}$, $(L/D)_2$, and $(L/D)_1$ may be taken from the appropriate table of reference 4 and substituted directly into equation (13) as a function of $\Delta\bar{V}$ (where $\Delta\bar{V} = 2 - \bar{V}$). Equation (13) may then be solved for the $(L/D)_{1V}$ of the flight vehicle and plotted as a function of velocity or the corresponding time (also given in the tables).

Although the above procedure is feasible, it was not directly followed for the example presented in figure 3; a new table of values was computed (from Chapman's equations) that resulted in a trajectory with a peak acceleration of precisely 10.0 g. This figure will be discussed in a later section.

Constant altitude phase.- For constant altitude flight the computation of the required $(L/D)_1$ is greatly simplified because both the reference flight-path angle γ_2 and $d^2(\bar{V}\gamma)/d\Delta\bar{V}^2$ are zero. Thus the required $(L/D)_{2V}$, evaluated from equation (9), is

$$\left(\frac{L}{D}\right)_{2V} = \frac{1 - \bar{V}_2^2}{\bar{A}_t/\sqrt{1 + (L/D)_2^2}} = \frac{4\Delta\bar{V} - \Delta\bar{V}^2 - 3}{\bar{A}_t/\sqrt{1 + (L/D)_2^2}} \tag{14}$$

When equation (14) is substituted into equation (13), the terms in the bracket will be identically zero and the equation will reduce to the simpler form:

$$\left(\frac{L}{D}\right)_{1V} = \frac{2\Delta\bar{V} - \Delta\bar{V}^2}{\bar{A}_t/\sqrt{1 + (L/D)_1}} - \frac{2\bar{A}_t(3 - \Delta\bar{V})}{\beta r[1 - \Delta\bar{V})(2 - \Delta\bar{V})]^2} \tag{15}$$

In equation (15) only the reference acceleration profile need be specified, which, for the constant altitude (ρ = const) segment, will vary as the square of the velocity:

$$\bar{A}_t = \bar{A}_{t_I}\left(\frac{\bar{V}}{\bar{V}_I}\right)^2 = \frac{\bar{A}_{t_I}}{\bar{V}_I^2}(2 - \Delta\bar{V})^2 \tag{16}$$

where $\bar{A}_{t_I}/V_I^2$ is a constant and is evaluated at pull out (maximum acceleration). Substituting equation (16) into (15) and simplifying yields

$$\left(\frac{L}{D}\right)_{1V} = \frac{\bar{V}_I^2\sqrt{1 + (L/D)_1^2}}{\bar{A}_{t_I}}\left(\frac{\Delta\bar{V}}{2 - \Delta\bar{V}}\right) - \frac{\bar{A}_{t_I}}{2\beta r}\left[\frac{3 - \Delta\bar{V}}{(1 - \Delta\bar{V})^2}\right] \tag{17}$$

The solution of equation (17) for the constant altitude portion along with (13) for the initial dive, comprises the approximate solution to the problem of matching the acceleration profiles of the two vehicles, one entering at planetary mission return velocity ($\bar{V}_i = 2$), the other at orbital return velocity ($\bar{V}_i = 1$). From this approximate solution a precise solution can be obtained on the analog computer.

The problem discussed earlier in specifying the nominal roll profile $\varphi(t)_{nom}$ in the vehicle control equation (eq. (4)) may now be resolved since a determination of the $(L/D)_{1V}$ profile is, in effect, a determination of the roll profile (since $\varphi = \cos^{-1}[(L/D)_V/(L/D)]$. An inconsistency exists here though, since the solution of equations (13) and (17) gives $(L/D)_{1V}$ as a function of the velocity variable $\Delta\bar{V}$ and not of the variable time. This is a problem for only the constant altitude portion of the trajectory since the tabulation of the reference trajectory variables in reference 4 for the initial dive includes the variable time. For the second phase of the entry trajectory a relatively simple relationship between time and $\Delta\bar{V}$ is derived in appendix B and is presented here.

$$t = \frac{(2 - \Delta\bar{V}_I)^2}{\bar{A}_{t_I}/\sqrt{1 + (L/D)_2^2}}\sqrt{\frac{r}{g}}\left(\frac{1}{2 - \Delta\bar{V}} - \frac{1}{2 - \Delta\bar{V}_I}\right) + t_I \tag{18}$$

The quantities $\bar{A}_{t_I}$, $\Delta\bar{V}_I$, and t_I are the acceleration, velocity change, and time, respectively, at initiation of the second phase (i.e., pull out). These values are numerically equivalent to those existing at the end of the initial dive. Using equation (18) in conjunction with equation (17) permits the evaluation of the nominal roll profile as a function of time. The profile in this form may be used in the control equation (eq. (4)) as the nominal roll profile.

Analog Computer Approach

The analytical step of the approach presented in the previous section gave an approximate solution for the L/D versus time (control) profile. To obtain this solution, it was assumed that the flight-path angle was small

and that the three vehicle translational equations were independent so that a solution based on a single differential equation of motion could be obtained. We shall now proceed with the more general analog computer step of the approach in which the above assumptions are not necessary.

For this step, the full set of the three differential equations was simulated on the computer. This allows a more precise solution for the control profile, provides flexibility for generating the desired reference trajectories, and permits evaluating the costs of performing the acceleration match (in terms of the sacrifice in vehicle ranging capability and changes in the aerodynamic heating on the vehicle). The set of differential equations in the form presented in the previous section (eqs. (1), (2), and (3)) are not suitable for direct programming on an analog computer. The large range of the program variables, plus the fact that the net radial acceleration is at times a small difference of large forces, presents scaling problems on the analog computer which greatly affect the accuracy of the results. However, if a more convenient axis system is introduced and the equation is modified to a perturbation form, the difficulties are reduced. The use of a modified flight-path axis system, introduced by Fogarty and Howe (ref. 3), will allow continuous simulation from orbital velocity and altitude through entry without rescaling. The modified equations in this form are presented in appendix C. The set of equations represents the three degrees of vehicle translational motion to which is added one degree of body rotational motion (roll axis) and additional auxiliary relationships to give the aerodynamic heating and to solve the vehicle control equation.

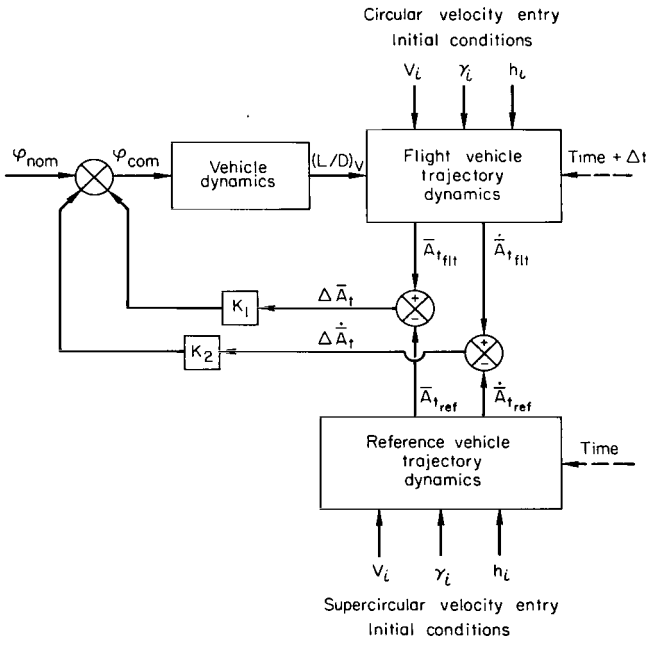

Figure 2.- Block diagram of analog computer study.

The analog computer set-up is represented diagrammatically in figure 2. The two large blocks represent the respective trajectory dynamics for the two vehicles. Two identical sets of the translational differential equations of motions were programmed on the analog computer. One set, representing the motions of the planetary mission entry vehicle, generates the reference trajectory state variables and removes the need for programming a precomputed reference. The second set represents the motion of the orbital mission entry vehicle. The two sets of equations are solved concurrently; thus, at each instant of time, the corresponding values of the state variables are available for comparison to give the error signal. The trajectory of the reference vehicle is completely independent, that is, different reference trajectory profiles are found through proper choice of the initial

conditions. The trajectory motions of the flight vehicle are related to those of the reference vehicle through the control equation (eq. (4)). The mechanization of the control equation is also shown in figure 2. The state variables generated by the trajectory dynamics are compared to obtain the error quantities ($\Delta\bar{A}_t$ and $\Delta\dot{\bar{A}}_t$); these are weighted appropriately (empirically) and summed with the nominal roll profile to obtain the commanded roll angle. The flight vehicle is commanded to roll so as to reduce the error quantities.

The approximate solution determined from the analytic step of the approach of the previous section was used as the initial estimate of the nominal control in the mechanized control equation. Since this control profile is only approximate, an error in the control parameters ($\Delta\bar{A}_t$, $\Delta\dot{\bar{A}}_t$) would develop even if no trajectory disturbances occurred. For the computer mechanization, provisions were available for manually adjusting the shape of the approximate nominal profile. By proper adjustment so that the magnitudes of the error quantities were reduced, a better approximation of the solution for the nominal control profile could be obtained. If the error quantities could be reduced to zero, then the true nominal and, consequently, the exact solution for the control would be found. The solution was not pursued to this extent since the lift required for certain regions of the control profile could not be achieved during the entry of an actual vehicle. Therefore, a compromise of the original objective of obtaining a precise match was required. The nature of this compromise will be explained fully in the next section.

DISCUSSION AND RESULTS

General Remarks

In the analysis section, an analytical expression (eq. (13)) was derived which gives an approximate solution for the control of a vehicle entering from orbit so that the acceleration profile that results would match that of a planetary mission vehicle entering the earth's atmosphere at twice orbital velocity. In this section, it will be shown that although it is impractical to obtain a precise match of the acceleration profile, an approximate match is obtainable and has certain advantages which will be expounded. This will be followed by an extensive discussion of the relationship that must exist between the orbital vehicle aerodynamics and trajectory characteristics and those of the planetary entry vehicle in order to obtain an approximate match. Finally, the cost of performing the acceleration match in terms of the resulting aerodynamic heating on the vehicle, the constraints on the vehicle maneuverability for range control, and the changes in the required velocity increment for the retro maneuver will be discussed.

Matching Considerations

In figure 3, a typical set of entry trajectories is presented for which the flight vehicle is controlled to generate the acceleration profile of the reference vehicle. The altitude, acceleration, and lift control profiles are presented as a function of the velocity variable $\Delta\bar{V}$. The reference

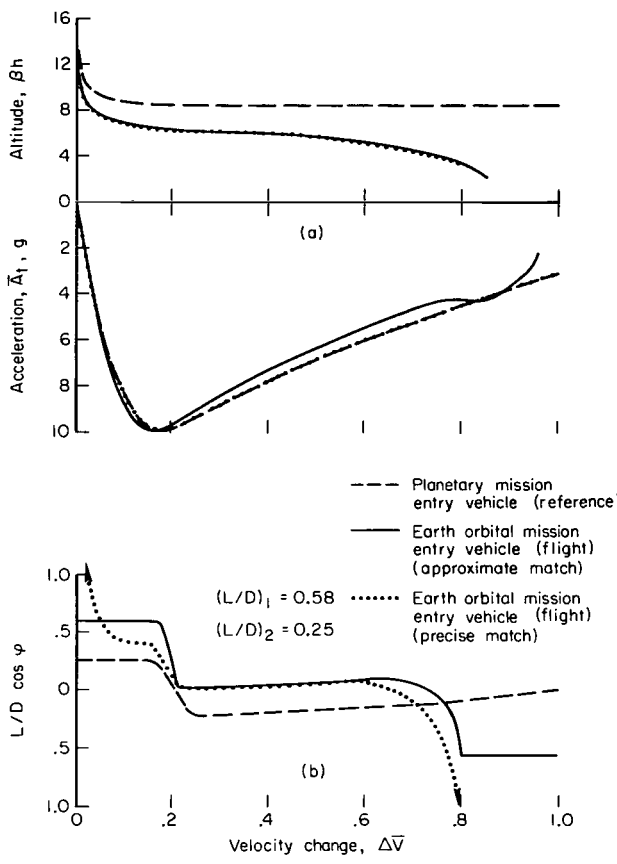

Figure 3.- Typical variation of earth entry trajectory parameters with velocity during planetary mission entry simulation.

acceleration profile has a peak of 10 g and could correspond to the entry of a planetary mission vehicle near the 10 g undershoot boundary. Figure 3 shows that the reference vehicle lift vector is up ($\varphi = 0^\circ$) during the initial dive (dashed curve), rolled over near peak acceleration to a downward direction to insure capture, and modulated for equilibrium during the subsequent period of constant altitude deceleration.

Two entries of the flight vehicle are illustrated. One entry is presented in which a precise acceleration match is achieved. This means that the acceleration is equal to the reference value at each point along the trajectory. Thus, the acceleration trace is identical to the reference acceleration trace (dash curve). The second entry represents an approximate match, which means that during the initial dive only the maximum values of $\bar{A}_t$ and $\dot{\bar{A}}_t$ are matched rather than the acceleration at each point. During the subsequent deceleration, the flight vehicle is controlled to achieve a close match of the reference acceleration profile in a closed-loop manner.

In figure 3, the profiles for the reference trajectory were generated by programming Chapman's entry equations on a digital computer. The control profile for the precise match is the quantitative solution of equation (13) using the outputs of $\bar{A}_t$, γ_2, and $\bar{V}_2$ from the digital program as the reference. The altitude profile is computed using equation (6) of the analysis section. Figure 3 shows that the L/D required for a precise match as computed from equation (13) is too large, at both the onset and end of the entry, to be achieved by the vehicle considered here. Although a precise match of the planetary mission entry acceleration profile by an earth orbital mission vehicle is physically unrealizable with a capsule-type configuration, because of the excessive aerodynamic lift required, the acceleration profile could be matched over portions of the entry. Figure 3 shows an example of this approximate match. The profiles for the approximate match were generated on an analog computer simulation of the entry with the same reference acceleration profile as that used to obtain the control profile for the precise match just described. Thus, this reference is also the dashed curve ($\bar{A}_t$ vs. $\Delta\bar{V}$) on figure 3. The approximate solution has the characteristics of matching the magnitudes of the peak acceleration and the peak acceleration rate during the

initial dive phase of the entry while the control profile retains the general shape of the control profile corresponding to the planetary mission entry trajectory. The approximate match is achieved with constant L/D (constant roll angle) during the initial dive, a roll-over maneuver at peak g, and then closed-loop control of the lift vector about the nominal during the subsequent period of acceleration. During the terminal portion of the entries ($\Delta\bar{V} > 0.5$) the magnitude of the roll angle progresses toward 90° (zero L/D) on fig. 3(b)) for the planetary mission entry, while for the orbital mission vehicle, the roll angle progresses toward 180° (negative L/D) as shown in figure 3(b). The difference in the two acceleration profiles in figure 3(a) is deceiving. Actually, the match on a time history plot is much closer than it appears here on a velocity history. The increasing error apparent in the two acceleration profiles as $\Delta\bar{V}$ increases reflects the inaccuracy in the assumption concerning $\Delta\bar{V}$ (i.e., $\Delta\bar{V}_1 = \Delta\bar{V}_2$) rather than the true difference in the time histories of the profiles. The time histories will be shown in later figures and the match will appear much closer.

Because the required lift is within the capability of the configuration and the small difference in the acceleration profile, the approximate match appears attractive and is studied to the exclusion of the other approach during the remainder of this report.

Computing the roll-angle profile of the flight vehicle requires the selection of an appropriate set of initial conditions for altitude, velocity, and flight-path angle, in addition to specifying the flight vehicle L/D. In the next section, we will discuss the manner in which these quantities are selected so that the maximum acceleration and maximum acceleration rate encountered during the initial dive into the atmosphere by the flight vehicle will match the respective value of the reference vehicle. It will then be shown that if the flight vehicle has the aerodynamic lift capability to match the initial dive portion of the acceleration profile of the planetary mission vehicle entry, then a match of the subsequent constant altitude deceleration portion is also within its capability.

Determination of Initial Conditions

A vehicle entering the earth's atmosphere will experience an acceleration buildup and a peak acceleration directly related to the initial velocity, flight-path angle, and vehicle lift-to-drag ratio. It can be shown that for a specified entry velocity and vehicle L/D, a unique correspondence exists between the peak acceleration rate and the peak acceleration encountered during the entries throughout a range of initial flight-path angles. This relationship between $\bar{A}_{t_{max}}$ and $\dot{\bar{A}}_{t_{max}}$ as a function of L/D is shown in figures 4(a) and 4(b) for two values of $\bar{V}_i$. These data were generated on the analog computer simulation of the initial dive. The peak values of $\bar{A}_t$ and $\dot{\bar{A}}_t$ were obtained during entries initiated at atmospheric encounter (the altitude at which 0.05 g is encountered) for a range of initial flight-path angles from -3° to -11°. Figure 4(a) presents these data for entries from earth orbit ($\bar{V}_i = 1$); figure 4(b) shows the same type of data for entries at twice the orbital velocity ($\bar{V}_i = 2.0$).

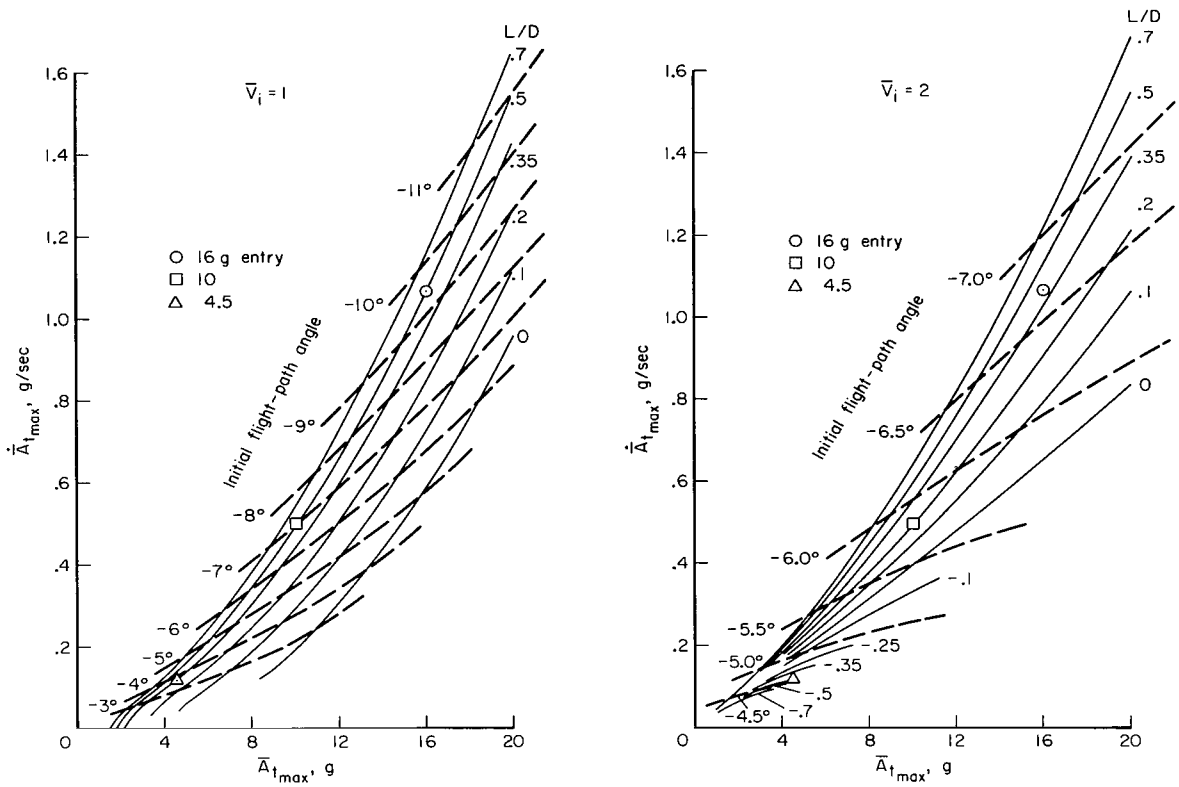

(a) Return from orbital mission.

(b) Return from planetary mission.

Figure 4.- Acceleration and rate of change of acceleration attained during earth entry.

For entries from earth orbit at constant L/D several acceleration peaks may occur during the course of the entry. Only the peak $\bar{A}_t$ and $\dot{\bar{A}}_t$ occurring during the first acceleration buildup are plotted in figure 4(a). Our interest is in matching the peak $\bar{A}_t$ and $\dot{\bar{A}}_t$ for the two types of entries. In certain regions $\bar{A}_{t_{max}}$ and $\dot{\bar{A}}_{t_{max}}$ for entries at $\bar{V}_i$ = 1 and 2 can be related through the variable L/D and the initial flight-path angle. Two entries, one at $\bar{V}_i$ = 1 (fig. 4(a)) and the other at $\bar{V}_i$ = 2 (fig. 4(b)), will achieve the identical peak $\bar{A}_t$ and peak $\dot{\bar{A}}_t$ if L/D and γ_i bear the relationship shown in figures 4(a) and 4(b). For example, to achieve an entry with a peak acceleration of 10 g and a peak acceleration rate of 0.5 g/sec requires that a vehicle entering at $\bar{V}_i$ = 2 have L/D = 0.2 and γ = -5.8° (from fig. 4(b)). A vehicle entering at $\bar{V}_i$ = 1 would require that L/D = 0.5 and γ = -7.0° (from fig. 4(a)). For this case, the orbital entry vehicle requires a greater aerodynamic lift capability than the planetary mission entry vehicle to achieve the identical peak $\bar{A}_t$ and $\dot{\bar{A}}_t$. For other cases, the L/D required may be less for the orbital entry vehicle than for the planetary mission entry vehicle. An example of this is an entry that achieves a peak $\bar{A}_t$ of 4.5 g and a peak $\dot{\bar{A}}_t$ of 0.12 g/sec. A vehicle entering at $\bar{V}_i$ = 2 requires that L/D = -0.5, while a vehicle entering at $\bar{V}_i$ = 1 requires that L/D = +0.35. The relationship between the lift requirements for a planetary mission type entry and the corresponding orbital mission entry that attains the same peak $\bar{A}_t$ and $\dot{\bar{A}}_t$ can be seen directly by cross-plotting the

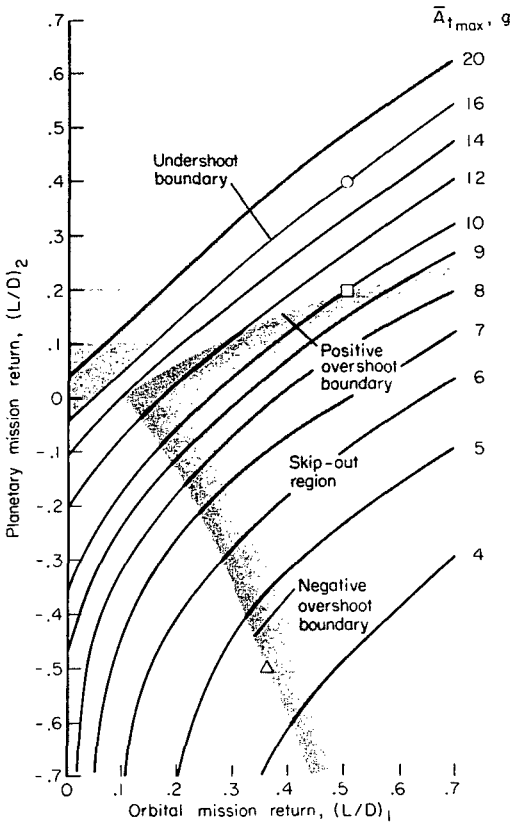

Figure 5.- L/D requirements for the initial dive phase.

$(L/D)_1$ and $(L/D)_2$ values of figures 4(a) and 4(b) for equivalent $\bar{A}_{t_{max}}$, $\dot{\bar{A}}_{t_{max}}$ pairs. The resulting variations are presented in figure 5. Each point on figure 5 represents two entries, one for the orbital mission return ($\bar{V}_i = 1$) and the other for the planetary mission return ($\bar{V}_i = 2$), both of which attain the identical peak acceleration and peak acceleration rate. The aerodynamic lift required during each entry is designated $(L/D)_1$ and $(L/D)_2$, respectively. Thus, from figure 5, the appropriate L/D can be established for an earth orbital mission vehicle so that it is possible to match the peak $\bar{A}_t$ and $\dot{\bar{A}}_t$ encountered during the initial dive portion of the planetary mission entry vehicle entry. The triangular shaded region on this plot represents entries in which the planetary mission entry vehicle does not enter the atmosphere sufficiently to be captured, but skips back out. Points along the border of this shaded region represent entries at the overshoot boundary. An overshoot boundary exists for entries at +L/D (lift vector up) as well as the more commonly understood negative overshoot boundary (-L/D, lift vector down). For entries at the positive lift overshoot boundary, the problems for vehicle control are compounded; for, in addition to skip out, there is an additional problem of exceeding the maximum allowable peak g. The vehicle enters with lift vector up ($\varphi = 0^\circ$) to keep the peak g within bounds. At pull out, a roll-over maneuver directs the lift vector downward ($\varphi = 180^\circ$) to attain capture. If the lift force is insufficient, the vehicle will skip back out of the atmosphere. For each entry of this type, there is a minimum allowable L/D to insure capture. These values of L/D and the corresponding peak acceleration define the +L/D overshoot boundary. For entry at the negative overshoot boundary, the peak accelerations will be low and of little concern. The vehicle enters with lift vector down ($\varphi = 180^\circ$) and retains this attitude through the pull out.

The undershoot boundary appears in figure 5 at the 16 g line. The undershoot boundary, which specifies the maximum allowable acceleration, was set arbitrarily at 16 g for this study, but could have been set at any reasonable value. A 10-g boundary is more commonly used. Two entry examples given earlier, one with $\bar{A}_{t_{max}} = 10$ g, the other with $\bar{A}_{t_{max}} = 4.5$ g, are represented in figure 5 by the square and triangular symbols, respectively. It is seen that the two examples actually represent entries at the positive and negative overshoot boundaries. An additional example at the 16-g undershoot

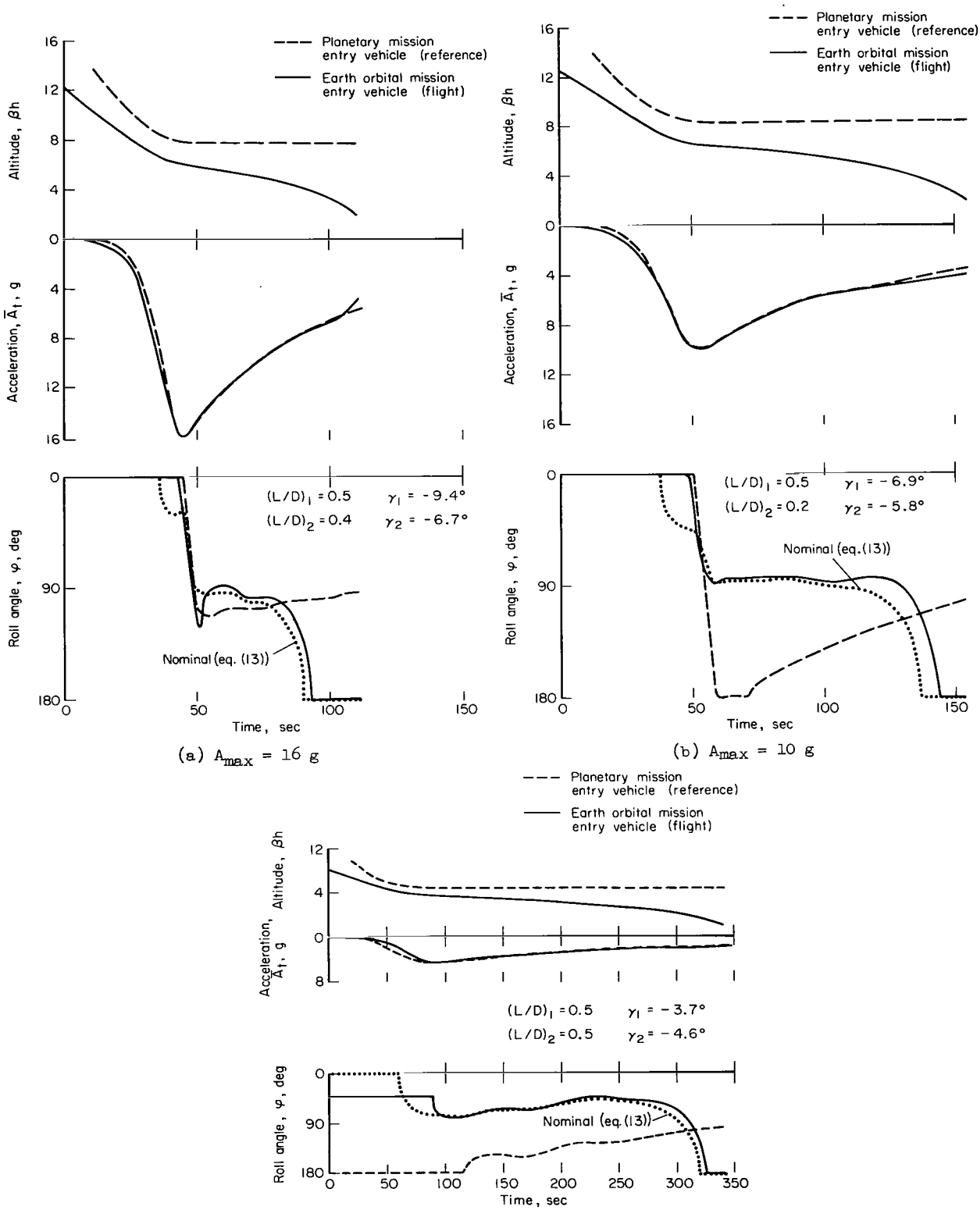

Figure 6.- Time histories of trajectory parameters during planetary mission entry simulation by earth orbital mission entry vehicle.

boundary is also indicated in figure 5 by the circular symbol. The figure shows that the acceleration profile of a planetary mission entry vehicle (L/D = 0.4) entering at the 16-g undershoot boundary may be duplicated by an earth orbital mission entry vehicle with L/D = 0.5. The appropriate initial flight-path angles for these entries are $\gamma_2 \approx -6.7$ and $\gamma_1 \approx -9.4$. The values of γ_i are determined from figures 4(a) and 4(b).

Results of the Matching Process

The three examples indicated in figure 5 will be used to illustrate the results of the matching process. The technique for matching the acceleration profiles was explained in the analog computer section of this report. The results of these entry simulations appear in figure 6, where the entries are shown from the time of atmospheric encounter until the flight vehicle reached an altitude of about 14.3 km (47,000 ft, $\beta h = 2$). This period corresponds to the initial dive phase and a portion of the constant altitude deceleration phase of the reference trajectory. The altitude, control, and acceleration profiles are shown as a function of time for the reference and flight vehicle. Zero time is chosen as the time at which the flight vehicle encounters an acceleration equal to 0.05 g.

In each figure, the altitude profile shows the flight vehicle diving initially to a lower, more dense altitude and remaining below the reference trajectory altitude throughout the entry. During the terminal phase, the flight vehicle dives progressively steeper into the atmosphere while the reference trajectory is a constant altitude.

The acceleration buildup is slightly more gradual for the flight vehicle than for the reference, which is characteristic of a slower vehicle. The magnitude and time of the acceleration peaks coincide. The acceleration rate peaks occur at approximately the same time and are of the same magnitude. (The point of occurrence of the peak acceleration rate is not readily discernible on these acceleration plots.) Good agreement between the acceleration profiles is achieved up to the point where the flight vehicle can no longer generate sufficient aerodynamic lift to pull down into the atmosphere at the progressively increasing rate required. Consequently, the flight vehicle acceleration profile diverges from the reference acceleration profile after this point, at about 94 seconds for the 16-g entry, 144 seconds for the 10-g entry, and 326 seconds for the 4.5-g entry.

The roll control profiles are shown in the lower portion of each figure. For the flight vehicle in each entry, L/D = 0.50. The L/D for the reference vehicle is 0.4, 0.2, and 0.5 for the 16-g, 10-g, and 4.5-g entry, respectively. In addition to the actual control profiles for the reference and flight vehicles, the nominal roll control profile for the flight vehicle is shown. These nominal roll control profiles (as explained before) are the quantitative solutions of equation (13) when the values of the planetary mission entry or reference vehicle state variables ($\bar{A}_t$, γ_2, and $(L/D)_2$) are used as the reference values. The control system of the flight vehicle attempts to control about this nominal. Excursions from the nominal are due, in part, to the closed-loop nature of the control and, in part, to the constraints on the

control action. One constraint limits the vehicle roll rate to less than $\pm 20^{\circ}$ per second. This caused a slight deviation of the control profile at roll over and during the terminal phase of the simulation where the nominal specifies a higher roll rate. An additional constraint does not allow the dip or discontinuity that appears in the nominal profile just prior to roll over in figures 6(a) and 6(b). This results in a smooth and continuous roll-over maneuver similar to that of the reference vehicle control profile instead of the discontinuous one specified by the nominal. The effect of this constraint on the acceleration profile is not noticeable.

Figure 6(c) shows the example time history for entry at the negative overshoot boundary. This case merits further discussion because it differs from the other two examples for entry at the positive overshoot and undershoot boundaries. During the initial dive, the flight vehicle enters with a roll angle of about 42°, indicating that the full lift capability of the vehicle is not required to achieve the match. This was not the situation for the other two examples which both required that the lift vector be full up ($\varphi = 0^{\circ}$) during the initial dive. It can be shown to be generally true that the $(L/D)_1$ required to simulate the entry at the negative overshoot boundary is less than the $(L/D)_2$ required for the actual planetary mission return entry. This can be verified from figure 5 for the example given here for $\bar{A}_{t_{max}} = 4.5$ g, as well as for many other examples that fall along the negative overshoot boundary. The opposite result (i.e., $(L/D)_1 > (L/D)_2$) is generally true at the positive overshoot and the undershoot boundaries.

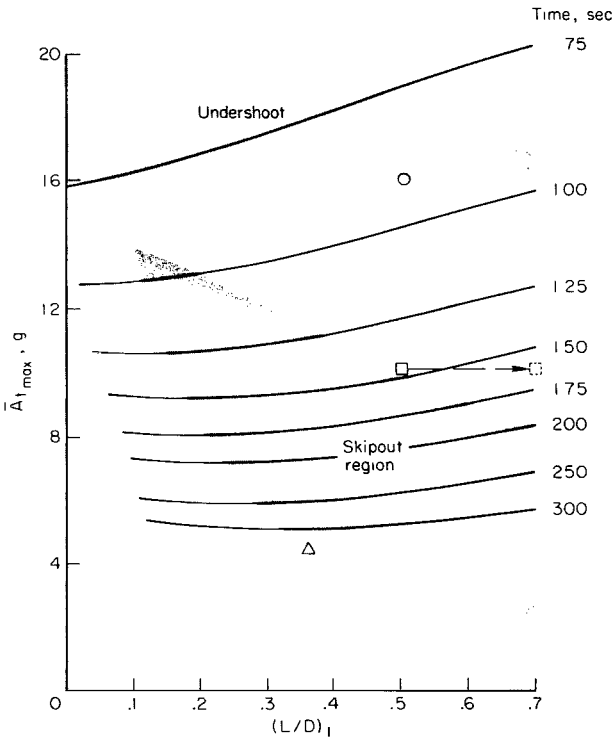

Figure 7.- Maximum duration of planetary entry simulation; time = 0 at $\bar{A}_t = 0.05$ g.

In figure 6(c) the shape of the flight vehicle roll control profile for entry at the simulated negative overshoot boundary does not resemble the control profile for the corresponding reference vehicle entry. There is, however, a close similarity in the shape of the reference and flight control profile for the other two cases (figs. 6(a) and 6(b)).

Simulation Time

The maximum time duration over which a simulated planetary mission entry may be sustained is presented in figure 7. Lines of constant time are given as a function of the peak acceleration encountered during the entry and the vehicle L/D. The values represent the total time from atmospheric encounter ($\bar{A}_t = 0.05$ g) until the flight vehicle can no longer sustain the desired level of acceleration. The

regions corresponding to the planetary mission return overshoot and undershoot trajectories are shown in this figure as was done in figure 5. The points corresponding to the three entry examples given previously (see figs. 5 and 6) are also included for reference.

It is apparent from the shallow slope of the curves that the time duration of the simulation is not a strong function of the vehicle L/D. For instance, a vehicle with an L/D of 0.50 could sustain a simulated planetary entry for 144 seconds for the $\overline{A}_{t_{max}}$ = 10 g case. This is indicated by the square symbol on figure 7. An increase in the vehicle L/D to 0.70 (40-percent increase) would result in an additional 20 seconds (14-percent increase) of simulation time for this 10-g case and would not affect the ability to attain a match during the high acceleration portion of the entry.

Aerodynamic Heating

For the entries from earth orbit considered in this study, only the aerodynamic heating that results when a laminar boundary layer is assumed will be evaluated. The Reynolds number can be shown to be less than 3×10^5 at peak heating for each of the entries of interest, making it reasonable to expect a considerable extent of laminar flow. The laminar convective heating rate per unit area at the stagnation point is given by

$$\dot{q} = K\sqrt{\rho}\, V^3$$

The constant K is selected so that the heating rate at peak heating matched that given by a presumably more accurate method of computation for the entry of the same configuration. In this study, the entry trajectory of the Apollo 204A mission was simulated on the analog computer using conditions as given in reference 5. The constant K was selected to match the peak heating rates for this entry. Results of the computations of the maximum heat rates and the total heat load defined as

$$H \equiv \int_0^t \dot{q}\, dt$$

are presented in figure 8 and compared with data obtained from reference 5. The orbital mission entry trajectories of interest in this study fall in a region near the origin in this plot. The three entry entry examples used previously are indicated within the region by the circle, square, and triangle for 16 g, 10 g, and 4.5 g, respectively. The peak heating rates and total heat loads experienced are much less than the capability of the Apollo capsule (lunar return configuration).

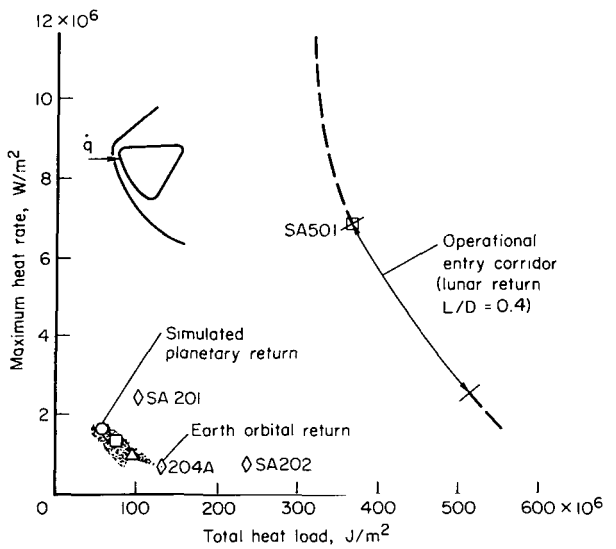

Figure 8.- Aerodynamic heating at the stagnation point.

The total heat loads are also less than the typical Apollo orbital flight 204A, although the heating rates are higher. Data points for Apollo flights SA201 and SA202 are also presented for comparison. These two flights are for ballistic lobs at higher entry velocities (28,500 ft/sec).

Range Control Considerations

During the entry from orbit, a spacecraft would perform range control maneuvers in order to arrive at a desired destination. Ideally, range error would be corrected most efficiently during the early portion of the entry where the maneuver capability of the vehicle is greatest. Performing range control during the early portion could conflict with the procedures required to fly the acceleration profile that was desired for the planetary entry simulation. To avoid this complication, control to achieve the desired acceleration profile and control to achieve a desired landing point are separated into two distinct phases in this study. A resulting decrease in range control capability will be one of the costs in performing this type of entry. Consider then that at some point during the entry, the planetary entry simulation will be terminated by the earth orbital mission return vehicle and terminal range control initiated. We will direct our attention to the effect simulation duration has on the range capability of the entry vehicle as specifically indicated by the size of the landing footprint. Using the previous example of the entry at the positive overshoot boundary that results in a maximum acceleration of 10 g, figure 9 shows the situation in which the control maneuver required to match the acceleration profile is terminated at a time prior to the absolute end point for the simulation. Three trajectories are shown in figure 9, two of which illustrate range control; the third trajectory is identical to the trajectory presented in figure 6(b). The trajectory designated ① indicates a situation in which the simulation is terminated after 80 seconds by rolling the vehicle so that the lift vector is up ($\varphi = 0^{\circ}$). This maneuver reduces the total acceleration on the vehicle as it rises in the atmosphere, and, ultimately, the vehicle is carried farther downrange. The second example (designated ②) indicates that the vehicle has rolled so that the lift vector is down. In this case, the vehicle dives deeper into the atmosphere, causing an increase in the acceleration and ultimately shortening the range to touchdown. During the analog computer analysis this procedure is carried out not only for the full-up and full-down direction of the lift vector, but for all directions between $\pm 180^{\circ}$ of roll angle. The trajectory that results for

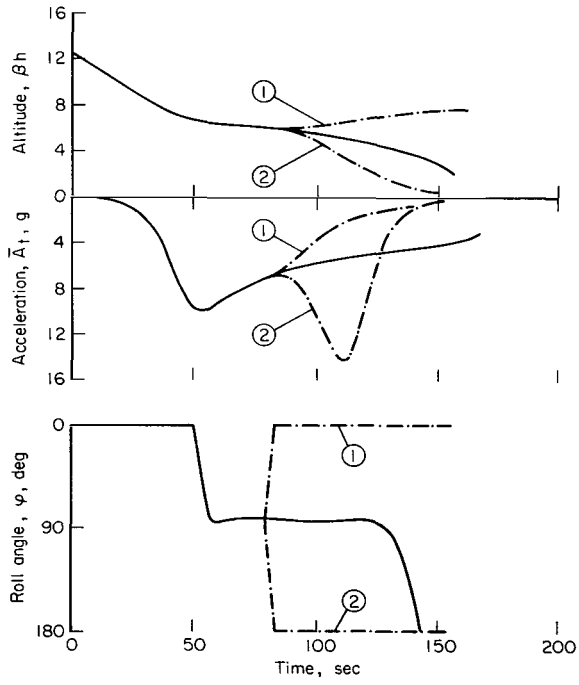

Figure 9.- Entry trajectory characteristics with range control; $\bar{A}_{max}$ = 10 g, L/D = 0.5.

each of the constant roll angle conditions is computed down to the terminal points (at 14.3 km, $\beta h = 2$), which are plotted to form a landing footprint as shown in figure 10. The footprint designated 80 seconds corresponds to the situation just described in which the simulation is terminated 80 seconds after entry. Progressively larger footprints would result if the simulation were terminated at earlier times, with the largest area representing the situation where there is no simulation at all ($t = 0$), and the ground area attainable is that resulting from using the maximum lift capability of the vehicle from the initial point at atmospheric encounter ($\bar{A}_t = 0.05$ g in these examples) down to the terminal point of 14.3 km altitude for each case.

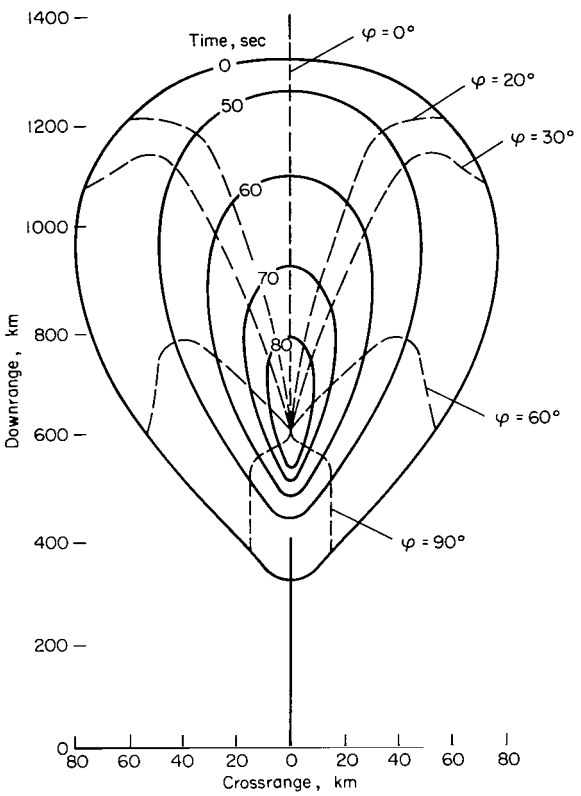

Figure 10.- Attainable ground area after termination of planetary_entry simulation of different durations; $A_{max} = 10$ g, $L/D = 0.5$.

For each trajectory in figure 10 the acceleration peak was at least 10 g and, for some of the trajectories in which the roll angle is greater than 90°, a second acceleration peak greater than 10 g (see ② on fig. 9) but always less than 20 g occurs.

It is apparent in figure 10 that there is a rapid decrease in footprint size or vehicle maneuver capability for simulation durations in excess of 50 seconds. This is readily apparent if the area of each footprint in figure 10 is determined and plotted as a function of simulation duration. In figure 11, these data are shown in dimensionless form for the 10-g case discussed here as well as for the cases that correspond to a 4.5-g entry and a 16-g entry (discussed previously). The high cost, in terms of loss in landing area available, for increased simulation time is indicated by the three curves in figure 11.

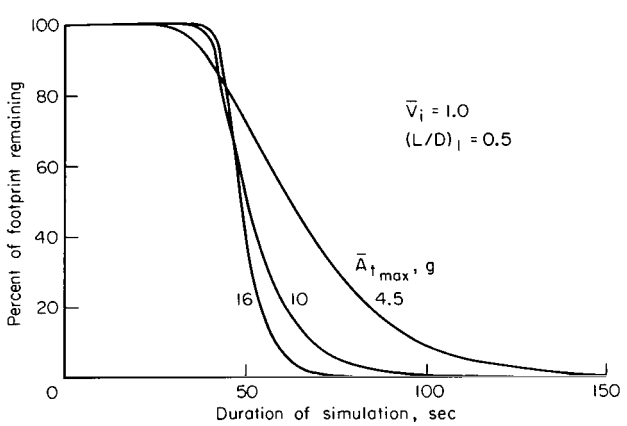

Figure 11.- Vehicle maneuver capability as a function of elapsed time from atmospheric encounter ($\bar{A}_t = 0.05$ g).

Midcorridor Entries

To illustrate the capability of an earth orbital mission vehicle to match the acceleration profile corresponding to the possible midcorridor entries of a planetary mission return vehicle, a summary plot similar to that in

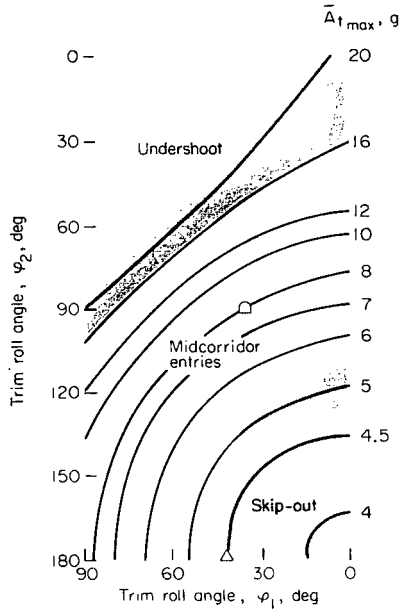

Figure 12.- Control requirements during initial dive for simulating midcorridor-type entries; $(L/D)_1 = 0.5$, $(L/D)_2 = 0.5$.

figure 5 of the control requirements for the initial dive portion is presented in figure 12. Figure 5 presented the capability for simulating entries at the overshoot and undershoot boundaries for different values of L/D, while the curves of figure 12 are for entries in the midcorridor range for only one value of L/D. Each point on the plot represents two entry trajectories, one for $\bar{V}_i = 2$, the other for $\bar{V}_i = 1$. Both trajectories attain the identical peak acceleration and peak rate of change of acceleration during the initial dive phase. Whereas entries at the undershoot and overshoot boundaries require the lift vector of the planetary mission entry vehicle to be either full up ($\varphi = 0^\circ$) or full down ($\varphi = 180^\circ$), the midcorridor type entries allow a component of the lift vector in the lateral plane. The vehicle roll attitude during the initial dive would still be constant but at a selected value between zero and $\pm 180^\circ$.

To obtain the data of figure 12, the flight and reference vehicle are both considered to have an L/D of 0.5. A slightly different plot would appear for each combination of $(L/D)_1$ and $(L/D)_2$. Figure 12 is for just one of these combinations.

The midcorridor entries on figure 12 are represented in terms of the peak acceleration attained and the roll attitude maintained by the reference vehicle, φ_2, and required of the flight vehicle, φ_1. The required flight-path angle for each vehicle has been omitted for the sake of clarity even though it is important in establishing the initial conditions.

As an example of the simulation of a midcorridor entry, consider a planetary mission vehicle entering the earth atmosphere at a roll attitude of 90° and at the appropriate flight-path angle for attaining a peak acceleration of 8 g. The peak acceleration and peak acceleration rate could be matched by an earth orbital mission vehicle entering at the appropriate flight-path angle with $\varphi_1 = 35^\circ$.

The example given previously corresponding to entry at the negative overshoot boundary is also indicated on figure 12 (triangle symbol). This is the entry example illustrated in figure 6(c), which attains a peak acceleration of 4.5 g.

Numerous other examples for simulation of midcorridor-type entries are within the capability of the orbital entry vehicle for the example given in

figure 12 [$(L/D)_1 = 0.5$, $(L/D)_2 = 0.5$]. All entries that fall between the two shaded regions on the plot represent feasible midcorridor entry simulations.

Retro Velocity Requirements

Thus far, no consideration has been given to how the entry vehicle arrived at the edge of the earth atmosphere flying at the correct flight-path angle to give the acceleration buildup and peak g anticipated. Under the assumptions that have been made for the initial dive into the atmosphere ($\bar{V}_i = 1$ and φ = constant), the peak g and maximum acceleration rate are a function of the L/D of the vehicle and the initial flight-path angle only. The proper L/D is determined as explained previously. The flight-path angle at entry will be a function of the initial orbit parameters and the retro velocity increment at the time of the deorbit maneuver.

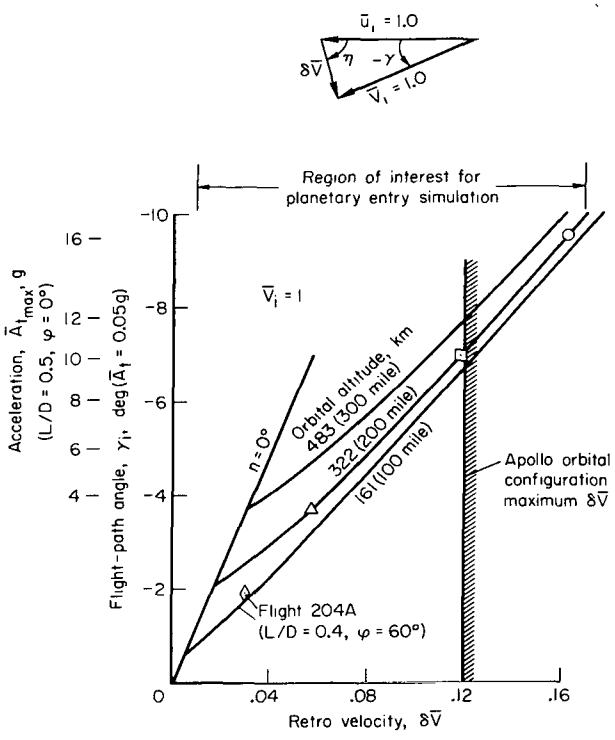

Figure 13.- Retro velocity requirements.

The curves presented in figure 13 show the relationship between the flight-path angle that would be realized at entry and the retro velocity increment added during the deorbit maneuver for three different initial orbital altitudes. On this plot it is possible to show a region of interest corresponding to planetary mission entry simulation and to compare this region with the available retro capability of the Apollo orbital vehicle. The vehicle is considered to be in a circular orbit prior to retro. The retro velocity increment is added in a direction to give the maximum negative flight-path angle when the vehicle arrives at the atmosphere.

A second ordinate axis is included on figure 13 to show the approximate peak acceleration that the vehicle would encounter upon entering with the lift vector up ($\varphi = 0^\circ$). The values $\bar{A}_{t_{max}}$ would be the lowest peak acceleration encountered for a designated γ_i. Higher peak accelerations could be encountered for entry at a roll angle greater than zero. The points corresponding to the three example entries are again included on this plot for trajectories from an initial orbital altitude of 322 km (200 statute miles).

It may be noted that for the 4.5 g example (triangle symbol) the vehicle does not enter with $\varphi = 0^\circ$ (see fig. 6(c)), and thus this data point does not relate to the acceleration ordinate on figure 13. For the other two examples, 16 g and 10 g, the roll angle is zero upon entry and the values given on the acceleration ordinate are correct.

The region of interest for planetary mission entry simulation is shown on the plot. Entries that result in peaks between 10 and 16 g, simulating entries at the undershoot boundary, show that large retro velocity increments are required in the range from $\delta\bar{V} = 0.12$ to $\delta\bar{V} = 0.17$ (950 to 1340 m/sec) for return from a 322-km orbit. The entries for midcorridor and overshoot boundary simulation ($\varphi > 0^{\circ}$) require smaller γ_i or $\delta\bar{V}$ and would extend the lower limit of the region of interest to include that shown in the figure ($\delta\bar{V} = 0.01$ to $\delta\bar{V} = 0.17$). It is noted that part of the region of interest lies beyond the capability of the present Apollo orbital configuration.

CONCLUSIONS

(1) The initial acceleration buildup (up to peak g) experienced during atmospheric entry of a planetary mission return vehicle may be duplicated during the entry of a manned earth orbital mission through proper choice of the lifting capability of the entering spacecraft and establishment of the appropriate initial flight-path angle. Accurate duplication of both the maximum acceleration and the maximum acceleration rate can be achieved for entries that simulate planetary return at the undershoot boundary, positive and negative lift overshoot boundaries, as well as midcorridor approach with a capsule-type spacecraft configuration.

(2) The acceleration profile corresponding to the constant altitude portion (after peak g) of a planetary mission return entry may be duplicated, in part, through proper control of the direction of the lift vector of the entering orbital spacecraft.

(3) The lift requirements for the orbital return vehicle are generally determined by the requirement to achieve a match of the acceleration profile during the initial dive into the atmosphere prior to peak g. The lift required to simulate the constant altitude portion of a planetary entry is generally less than this initial segment. Only small and inefficient gains result from increasing the vehicle lift capability above that required during the initial dive in order to increase the duration of the simulation of the constant altitude segment.

(4) Downrange and crossrange capabilities are reduced by control maneuvers required to achieve the acceleration profile match. The subsequent reduction in the size of the vehicle landing footprint is a strong function of the velocity (or time) at which the simulation is terminated and range control initiated.

(5) Large entry flight-path angles, implying large retro velocity increments, are required by the orbital-type entry vehicle to simulate a high g planetary mission entry at the undershoot boundary. Lower retro velocity increments are required for simulating midcorridor and overshoot boundary type entries.

Ames Research Center
National Aeronautics and Space Administration
Moffett Field, Calif., 94035, June 14, 1968
125-19-01-42-00-21

APPENDIX A

CONDITIONS FOR USING EQUATION (8)

To obtain a quantitative solution of equation (13) in the analytic section, we have considered that the total velocity change experienced by the reference and flight vehicles during the entries was identical at corresponding times along the trajectories and, further, that this total velocity change was equal to the integral of the total acceleration vector:

$$\int \bar{A}_{t_2}\, dt = \int \bar{A}_{t_1}\, dt \qquad \text{or} \qquad \Delta V_2 = \Delta V_1 \tag{A1}$$

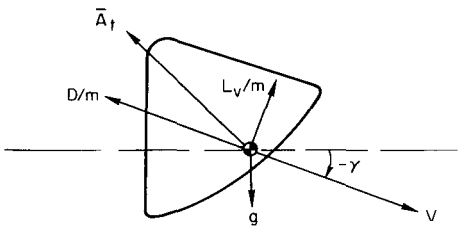

Sketch (a).

In sketch (a) the change in total velocity for each vehicle is

$$\Delta V = \left(\frac{-D}{m} + g \sin \gamma\right) \Delta t \tag{A2}$$

or, in dimensionless integral form,

$$\Delta \bar{V} = \int_0^{\tau} \left(\frac{-\bar{A}_t}{\sqrt{1 + (L/D)^2}} + \sin \gamma\right) d\tau' \tag{A3}$$

where the drag acceleration has been replaced by the equivalent value in terms of the total acceleration $\bar{A}_t = (D/mg)\sqrt{1 + (L/D)^2}$.

From equation (A3) in order for the velocity change to be equal for the two vehicles, a unique correspondence must exist between the flight parameters $\bar{A}_t$, L/D, and γ for the two vehicles. Since the flight vehicle is controlled so that the acceleration $\bar{A}_{t_1}$ is equal to the reference value $\bar{A}_{t_2}$ at each point along the trajectory, it is apparent that an error would develop if an inequality exists in the values of $(L/D)_1$, $(L/D)_2$, γ_1, and γ_2. This error would be

$$\text{Error} = \int_0^{\tau} -\bar{A}_t \left[\frac{1}{\sqrt{1 + (L/D)_2^2}} - \frac{1}{\sqrt{1 + (L/D)_1^2}}\right] + (\sin \gamma_2 - \sin \gamma_1) d\tau' \tag{A4}$$

Although it is feasible to have $(L/D)_1 = (L/D)_2$, it should be clear that the flight-path angles could not be equivalent at each point along the trajectory (see altitude time histories, fig. 6). Thus an error will always develop as a result of this difference in flight-path angles. Depending on the particular trajectory flown, this error in $\Delta \bar{V}$ may vary from 2 to 9 percent of the total velocity change at the end of simulation. This error will have only a small effect on the acceleration matching results.

APPENDIX B

TIME EQUATION

An approximate equation may be derived that relates the accumulated time along the entry trajectory with the velocity change for the constant altitude portion of the entry. For the constant altitude phase of the reference vehicle entry ($\gamma \approx 0^{\circ}$ and ρ = const), equation (A2) reduces to

$$\Delta V = -\frac{D}{m}\Delta t \tag{B1}$$

from which the change in time can be related directly to the change in velocity as

$$t - t_I = \sqrt{\frac{r}{g}} \int_{V_I}^{V} \frac{d\bar{V}}{\bar{A}_t / \sqrt{1 + (L/D)^2}} \tag{B2}$$

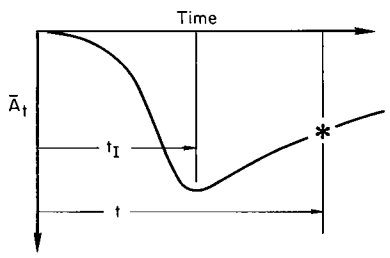

Sketch (b).

where the limits of integration extend from the velocity at initiation of the constant altitude phase (pull out) to the point of interest along the trajectory (designated * in sketch (b)).

For this constant altitude phase (constant atmospheric density), the total acceleration varies as the square of the velocity.

$$\bar{A}_t = K\bar{V}^2 \qquad \text{where} \qquad K = \frac{\bar{A}_{t_I}}{\bar{V}_I^2} \tag{B3}$$

Thus, we can substitute for the acceleration and obtain an expression that can be integrated:

$$t - t_I = \sqrt{\frac{r}{g}} \frac{\sqrt{1 + (L/D)_2^2}}{K} \int_{\bar{V}_I}^{\bar{V}} \frac{d\bar{V}}{\bar{V}^2} \tag{B4}$$

After integrating and substituting the limits, we obtain

$$t = \sqrt{\frac{r}{g}} \frac{\sqrt{1 + (L/D)_2^2}}{K} \left(\frac{1}{\bar{V}} - \frac{1}{\bar{V}_I}\right) + t_I \tag{B5}$$

or, in terms of the independent variable $\Delta\bar{V}$ for an initial velocity of $\bar{V}_2 = 2$,

$$t = \sqrt{\frac{r}{g}} \frac{\sqrt{1 + (L/D)_2^2}}{K} \left(\frac{1}{2 - \Delta\bar{V}} - \frac{1}{2 - \Delta\bar{V}_I}\right) + t_I \tag{B6}$$

APPENDIX C

EQUATIONS OF MOTION

Equations for the angular and translational motions of the spacecraft (three translational degrees of freedom and one rotational degree about the roll axis) are given herein. The equations are given in terms of a modified flight-path axis system (H frame) that is rigidly attached to the vehicle and moves with it. The three translational equations (from ref. 3) are

$$\dot{U}_h - \frac{U_h W_h}{r} = \frac{X_h}{m}$$

$$\dot{\psi} U_h = \frac{Y_h}{m} \qquad \text{(motion is in equatorial plane)}$$

$$\dot{W}_h + \frac{U_h^2}{r} - g_o \left(\frac{r_o}{r}\right)^2 = \frac{Z_h}{m}$$

where U_h and W_h are the vehicle velocity components in the H frame and $V_h = 0$ by definition of the H frame (see ref. 3).

To simplify the equations with respect to computer scaling, the following dimensionless variables are introduced:

$$\Delta\rho = \frac{r}{r_o} - 1 \qquad \text{(altitude)}$$

$$\Delta u_h = \frac{U_h - U_{h_o}}{\sqrt{g_o r_o}} ; \qquad w_h = \frac{W_h}{\sqrt{g_o r_o}} \qquad \text{(velocity)}$$

$$\tau = \sqrt{\frac{g_o}{r_o}}\, t \qquad \text{(time)}$$

In terms of these new variables, the translational equations of motion become

$$\Delta u_h = \frac{1}{1 + \Delta\rho}\left[\int_o^\tau (1 + \Delta\rho)\, \frac{X_h}{m g_o}\, d\tau' - \Delta\rho\right]$$

$$\psi_h = \int_o^\tau \frac{1}{1 + \Delta u_h}\, \frac{Y_h}{m g_o}\, d\tau'$$

$$w_h = \int_o^\tau \left[\frac{\Delta\rho}{(1 + \Delta\rho)^2} - \frac{2\Delta u_h + (\Delta u_h)^2}{1 + \Delta\rho} - \frac{Z_h}{m g_o}\right] d\tau'$$

The external forces on the vehicle (not including gravity) are

$$\frac{X_h}{mg_o} = \frac{D}{mg_o}\left(-\frac{L}{D}\sin\gamma + \cos\gamma\right)$$

$$\frac{Y_h}{mg_o} = -\frac{L}{D}\left(\frac{X_h}{mg_o}\right)\sin\varphi$$

$$\frac{Z_h}{mg_o} = \frac{D}{mg_o}\left(\frac{L}{D}\cos\gamma + \sin\gamma\right)$$

where the flight-path angle γ is defined as

$$\gamma = \tan^{-1}\left(-\frac{W_h}{U_h}\right)$$

The total acceleration and rate of change of acceleration is

$$\bar{A}_t = \frac{D}{mg_o}\sqrt{1 + \left(\frac{L}{D}\right)^2_{max}}$$

$$\dot{\bar{A}}_t = \bar{A}_t\left(\frac{2}{\beta}\frac{D/mg_o}{\sqrt{U_h^2 + W_h^2}} - W_h\right)$$

Auxiliary relationships are:

$$\text{Total velocity} = (U_h^2 + W_h^2)^{1/2}$$

$$\text{Downrange} = \int_o^\tau (1 + \Delta u_h)\cos\psi_h \, d\tau'$$

$$\text{Crossrange} = \int_o^\tau (1 + \Delta u_h)\sin\psi_h \, d\tau'$$

REFERENCES

1. Wingrove, R. C.: Flight Dynamics of Planetary Entry. Presented at AAS/AAAS Special Astronautics Symposium, December 29, 1965.

2. Chapman, Dean R.: An Approximate Analytical Method for Studying Entry Into Planetary Atmospheres. NASA TR R-11, 1959.

3. Fogarty, L. E.; and Howe, R. M.: Flight Simulation of Orbital and Reentry Vehicles. Part II - A Modified Flight Path Axis System for Solving the Six-Degree-of-Freedom Flight Equations. ASD TR 61-171 (II), Oct. 1961.

4. Chapman, Dean R.; and Kapphahn, Arline K.: Tables of Z Functions for Atmosphere Entry Analyses. NASA TR R-106, 1961.

5. Strouhal, G.; Curry, D. M.; and Janney, J. M.: Thermal Protection System Performance of the Apollo Command Module. Presented at the AIAA/ASME Seventh Structures and Materials Conference, April 18-20, 1966.

NASA-Langley, 1968 —— 31 A-2923

NATIONAL AERONAUTICS AND SPACE ADMINISTRATION
WASHINGTON, D. C. 20546

OFFICIAL BUSINESS

FIRST CLASS MAIL

POSTAGE AND FEES PAID
NATIONAL AERONAUTICS AND
SPACE ADMINISTRATION

POSTMASTER: If Undeliverable (Section 158 Postal Manual) Do Not Return

"The aeronautical and space activities of the United States shall be conducted so as to contribute . . . to the expansion of human knowledge of phenomena in the atmosphere and space. The Administration shall provide for the widest practicable and appropriate dissemination of information concerning its activities and the results thereof."

—NATIONAL AERONAUTICS AND SPACE ACT OF 1958

NASA SCIENTIFIC AND TECHNICAL PUBLICATIONS

TECHNICAL REPORTS: Scientific and technical information considered important, complete, and a lasting contribution to existing knowledge.

TECHNICAL NOTES: Information less broad in scope but nevertheless of importance as a contribution to existing knowledge.

TECHNICAL MEMORANDUMS: Information receiving limited distribution because of preliminary data, security classification, or other reasons.

CONTRACTOR REPORTS: Scientific and technical information generated under a NASA contract or grant and considered an important contribution to existing knowledge.

TECHNICAL TRANSLATIONS: Information published in a foreign language considered to merit NASA distribution in English.

SPECIAL PUBLICATIONS: Information derived from or of value to NASA activities. Publications include conference proceedings, monographs, data compilations, handbooks, sourcebooks, and special bibliographies.

TECHNOLOGY UTILIZATION PUBLICATIONS: Information on technology used by NASA that may be of particular interest in commercial and other non-aerospace applications. Publications include Tech Briefs, Technology Utilization Reports and Notes, and Technology Surveys.

Details on the availability of these publications may be obtained from:

SCIENTIFIC AND TECHNICAL INFORMATION DIVISION

NATIONAL AERONAUTICS AND SPACE ADMINISTRATION

Washington, D.C. 20546